Carbon Resources Conversion 8 (2025) 100301

Contents lists available at ScienceDirect

Carbon Resources Conversion

journal homepage: www.keaipublishing.com/en/journals/carbon-resources-conversion

Original Article

Mesoporous carbon derived from lignin sulfonate as a sustainable cathode for high-performance aluminium batteries

Fathima Ali Kayakool [a,c], Harita Pant [a,c], Menestreau Paul [e], Glaydson Simões Dos Reis [b,c], Gopinathan Manavalan [c,d], Vadali Venkata Satya Siva Srikanth [a,*], Mikael Thyrel [c], Shaikshavali Petnikota [c,*]

[a] School of Engineering Sciences and Technology, University of Hyderabad, Gachibowli, Hyderabad 500046, Telangana, India
[b] Laboratory of Industrial Chemistry and Reaction Engineering, Faculty of Science and Engineering, Åbo Akademi University, 20500 Åbo/Turku, Finland
[c] Biomass Technology Centre, Department of Forest Biomaterials and Technology, Swedish University of Agricultural Sciences, SE-90183 Umeå
[d] Technical Chemistry, Department of Chemistry, Chemical-Biological Centre, Umeå University, SE-90187 Umeå, Sweden
[e] Public Research University Engineering School, IMT Mines Albi, Albi 81000, France

ARTICLE INFO

Keywords:
Lignin sulfonate
Paper and pulp industry
Mesoporous carbon
Cathode materials
Aluminium batteries

ABSTRACT

The development of sustainable and efficient energy storage systems is crucial for addressing the growing global energy demand. This study investigates the potential of mesoporous carbon derived from lignin sulfonate as a cathode material for aluminium batteries. Lignin sulfonate, a by-product of the paper industry, was used as a precursor to synthesize mesoporous carbon through a facile and eco-friendly activation process. The resulting carbon material exhibited a high specific surface area of ~ 2259 m^2/g and a well-defined balance of micro- and meso- porosity, making it a promising cathode material for high-performance aluminium batteries. Electrochemical characterization showed that the mesoporous carbon cathode delivered an impressive specific capacity of 91 mAh/g at 1.0 A/g current density even after 7000 cycles with excellent cycling stability. It delivered superior rate capabilities of 105, 89, 80, 72, 67, 63, 90, and 105 mAh/g at 0.1, 1.0, 2.0, 3.0, 4.0, 5.0, 1.0, and 0.1 A/g current rates, respectively. The use of lignin-sulfonate as a precursor to prepare mesoporous carbon opens up a new sustainable way for improving the electrochemical performance of carbon-based cathode materials for aluminium batteries.

1. Introduction

Lithium-ion batteries (LIBs) have attained stunning success in modern society with the revolution of mobile electronic devices and electric vehicles. Despite LIBs' spectacular commercial adaptation and being the frontrunner among all rechargeable batteries, the future of LIBs is still uncertain due to the severe deposit shortages of lithium and other LIB materials such as nickel and cobalt [1]. Hence, pushing for new battery developments that are safe, low cost, and have high energy density is mandatory. In this context, aluminium (Al) battery technology has emerged as a potential alternative energy storage system due to its many advantages over commercial LIBs. Firstly, Al is much cheaper and more abundant than Li. Moreover, Al^{3+} has a theoretical specific capacity of 2980 mAh/g, very competitive to Li^{+} (3870 mAh/g); In addition, its volumetric specific capacity is 8050 mAh/cm^3, higher than Li and other metal electrodes [2–4]. Thus, due to these advantages, Al-batteries (ABs) can be used as suitable candidates for cost-effective and high-energy density batteries for both portable electronic devices and large-scale stationary applications. However, the successful development of ABs is highly dependent on the cathode part, and it became the limiting factor and bottleneck that stalls ABs' practical application. Some materials have been investigated as cathodes for ABs, including graphite [5–7], metal oxides [3,8–10], vanadium phosphates [9], graphene [2,11–13], and biomass carbon materials [14]. However, these materials are very costly and present highly complex synthesis routes, which has sparked the need for more sustainable materials for high-performance and greener ABs. Moreover, as graphite is considered one of the most promising cathode materials for ABs, it also faces severe issues regarding the intercalation of large $AlCl_4^-$ anions (~0.528 nm) into its narrower interlayer spacing (~0.335 nm), which results in poorer charge storage process [7]. In addition, this intercalation issue may result in severe volume expansion, damaging the graphite host structure after a few

* Corresponding authors.
E-mail addresses: vvsssse@uohyd.ac.in (V.V.S.S. Srikanth), shaikshavali.petnikota@slu.se (S. Petnikota).

https://doi.org/10.1016/j.crcon.2024.100301
Received 10 August 2024; Received in revised form 4 November 2024; Accepted 31 December 2024
Available online 3 January 2025

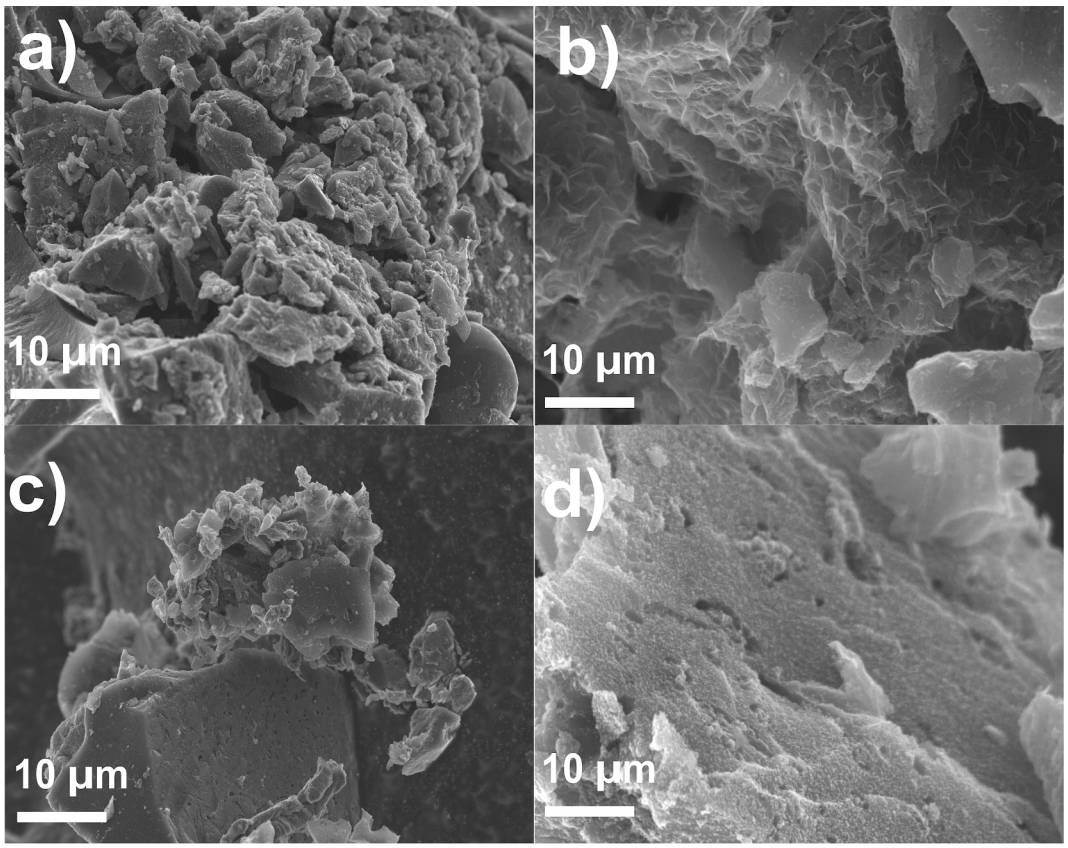

Fig. 1. SEM images of a) LS-C-1:2, b) LS-C-1:2, c) LS-C-1:4, and d) LS-C-1:4 samples at different magnifications.

cycles [2,15]. Biomass-based carbon materials appear suitable, sustainable, and high-performance cathode materials for ABs due to their good physicochemical properties [14]. Activated biochar can be easily prepared from any kind of biomass resources [16,17] and they have suitable features for $AlCl_4^-$ intercalation such as high specific surface area, well-developed pore structure as well as stable chemical surface properties. In addition, compared to the aforementioned cathodes, biomass-based cathodes would be both environmentally friendly and economically advantageous, opening up new possibilities for producing green, low-cost, and high-capacity Al-based battery systems [14,16].

In this work, we used lignin sulfonate (LS) as a biomass precursor for producing high-performance cathodes for Al-battery. LS is one type of lignin, a by-product from the paper industry [18], and part of the second most naturally abundant biomass resource (lignin) after cellulose [16]. The annual production of lignin materials is approximately 7000 tons [19], with only ~5 % of them being used in value-added applications [20]. As far as we know, there are no studies that report using lignin-based materials (example, LS) to produce cathode materials for ABs. Here, we present a comprehensive study that considers LS as a carbon precursor to produce high specific area carbons and test their applicability as the potential cathode materials for AB. Two cathode materials with different pore structures were evaluated regarding their electrochemical performances. Our study revealed that the porosity features of the cathodes had implications on their electrochemical performance metrics and that the as-derived (from LS) carbon cathodes with 3D network structure could facilitate electron and Al-ion transport. The good carbon network stability may have helped to alleviate the volume changes. Therefore, the ABs with LS-derived carbon cathodes exhibited good cycling stability. As a result, a reversible capacity of 91 mAh/g was achieved after 7000 cycles at 1000 mA/g. Thus, it can be considered that LS-derived carbon is an above-par cathode material for Al-battery application. Moreover, this work gives the first insights into using an easy and effective strategy to make high-performative biomass-based cathode materials. Therefore, we expect this work to open up new strategies for the fabrication/development of high-performance cathodes for ABs.

2. Experimental Section

The LS-derived carbons were prepared using a one-step pyrolysis activation process [21,22]. Initially, 20 g of LS precursor was mixed with KOH at two different ratios (1:2 and 1:4), and approximately 40 mL of water was added during blending to ensure uniform formation of the paste. It may be noted that LS precursor: KOH ratios > 1:4 did not yield homogeneous mixtures. Subsequently, the pastes were dried in an oven set at 105 ℃ for 24 h, followed by pyrolysis in a reactor externally heated by an electric oven. The pyrolysis process was conducted at 900 ℃ at a constant heating rate of 10 ℃/min for 1 h and under an inert atmosphere (N_2 flow of 50 mL/min). Upon reaching the designated temperature, the sample was held at that temperature for 1 h. The reactor was allowed to cool down to room temperature. To eliminate any residual KOH, the samples were subjected to several washing processes with boiling water until the pH of the supernatant was kept constant (close to neutral) [23,24]. The two samples were named LS-C-1:2 (LS:KOH ratio of 1:2) and LS-C-1:4 (LS:KOH ratio of 1:4).

The surface morphology was observed on a Carl Zeiss Merlin field-emission scanning electron microscopy (FE-SEM) operated at 5 kV. The BET-specific surface area, pore size, and pore volume of the LS-derived carbon powders were determined by liquid nitrogen (N_2) physisorption using a Micromeritics TriStar 3000 porosimeter. Adsorption-desorption isotherms were recorded at –196 ℃ after the powders were degassed at 110 ℃ for 2 h. Raman spectra of the LS-derived carbons were recorded with a 532 nm solid-state laser on a Renishaw Qontor spectrophotometer with a confocal microscope. The structural characterization was done using X-ray diffraction (XRD) analysis. XRD patterns of the samples were recorded using Bruker D8 X-

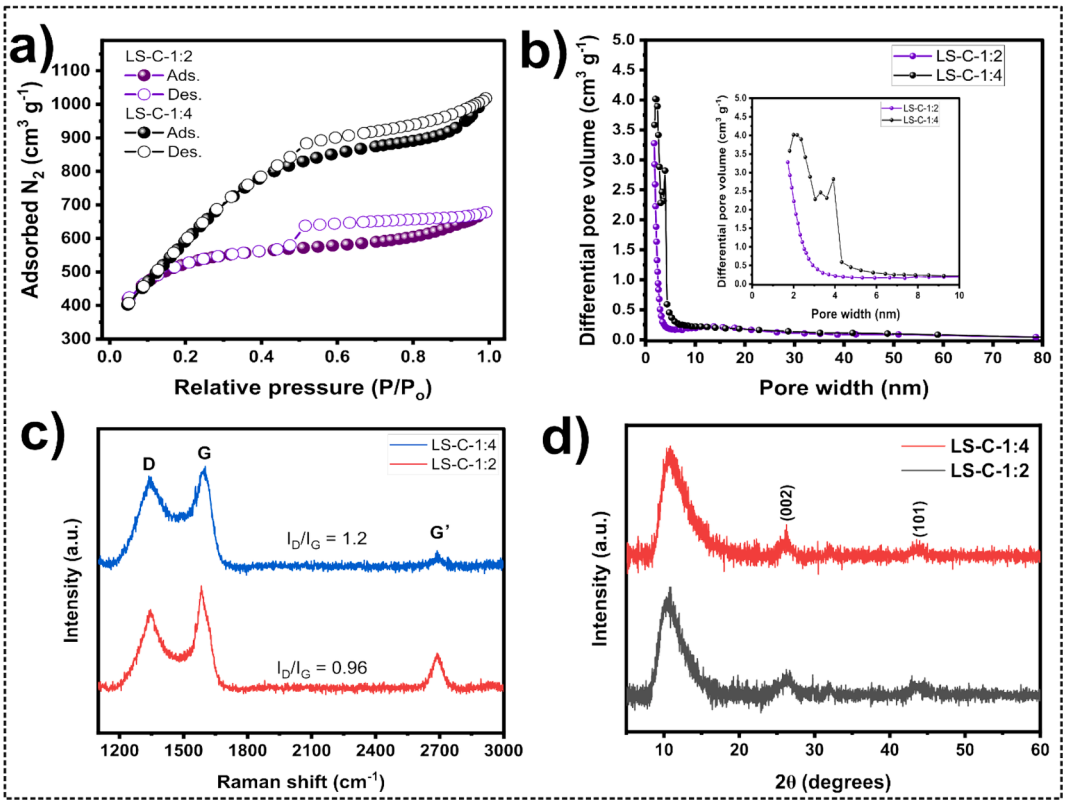

Fig. 2. a) N_2 adsorption-desorption isotherms, b) Pore size distribution curves, (c) Raman spectra, and (d) XRD patterns of LS-C-1:2 and LS-C-1:4 samples.

ray diffractometer, over a 2θ range of 5–60° using a Cu Kα radiation source (λ = 1.54 Å). The step size was set to 0.02° to ensure recording of high-resolution data. The obtained XRD data were analyzed using standard procedures. Morphological analysis was also done using transmission electron microscope (TEM). The sample preparation for TEM was done by finely grinding the sample to achieve a uniform particle size, and a small amount of the ground sample was dispersed in ethanol using an ultrasonic bath for 10–15 min to ensure a homogenous suspension. A drop of the suspension was placed on a copper grid coated with a carbon film. The grid was dried at room temperature to evaporate the ethanol. The prepared sample on the copper grid was loaded into the TEM (Jeol JEM F200). High-resolution images were captured to analyze the morphology and structure of the particles.

The electrochemical analysis was conducted by preparing pouch cells, which were tested using a BioLogic 800 series battery cycler and BioLogic SP-150e potentiostat. Separate tests were conducted on LS-C-1:2 and LS-C-1:4 as the AB cathodes. Slurries of LS-C-1:2 and LS-C-1:4 were prepared by mixing 80 wt% active material with 10 wt% NaCMC from (Sigma Aldrich) and 10 wt% carbon black (Super P Carbon) in a 1:1 ethanol and water solution. The resulting slurries were drop-cast onto molybdenum foil (≥99.9 %, 0.1 mm thick, Sigma Aldrich) and dried in a hot air oven at 105 ℃ following well-reported procedures [25]. Pouch cells were assembled using the coated electrodes as the cathode, aluminium (0.25 mm thick, 99.999 %, Advent Research Materials Ltd) as the anode, glass microfiber filters (Whatman GF/D) as the separator, and molybdenum foil as the current collecting tabs. The AB pouches were assembled inside an Ar-filled glove box by sealing the electrodes and separator inside aluminium laminated film casings. The 1.3 M $AlCl_3$: [EMIM]Cl electrolyte of about 300–500 μL was added before sealing the pouches. More details about the pouch cell fabrication and electrolyte preparation can be found in our recent publications [2,3,13]. The cyclic voltammetry (CV) of LS-derived carbons was carried out with BioLogic SP-150e potentiostat at a scan rate of 1.0 mV/s whilst charge–discharge and rate performance were recorded with current densities in the range of 0.1 to 5.0 A/g using BioLogic 800 series battery cycler. An operating voltage of 0.01 – 2.2 V was considered for all the battery tests.

3. Results and Discussion

3.1. Morphological, structural, specific surface area and pore characteristics of the LS-derived carbons

SEM analysis was carried out to evaluate the morphological features of the LS-derived carbons (Fig. 1). The SEM images of LS-C-1:2 and LS-C-1:4 displayed distinct morphologies, LS-C-1:2 exhibited much more irregular surfaces, some similar small flake structures with evident defects, which seems to be a notably more porous and rougher three-dimensional matrix compared to LS-C-1:4. Unlike, LS-C-1:2, LS-C-1:4 exhibited what it seems to be less rough surface with less irregularity (at lower magnification, Fig. 1c), however, at higher magnification (Fig. 1d), the surface shows to be extremely rough with huge presence of small pores. The exhibition of highly rough surfaces indicates the formation of a well-developed porosity caused by chemical etching and gasification during KOH activation and carbonization at high temperatures, which results in very high specific surface areas.

Among all the essential cathode material characteristics of ABs, the porosity features, such as specific surface area and pore structure, usually influence the cathode electrochemical performance [14]. Hence, N_2 adsorption and desorption isotherms and pore size distribution data of the LS carbons are shown in Fig. 2 to evaluate their porosity characteristics properly. Fig. 2a displays similar curve behaviors. According to the IUPAC classification [26], both isotherms could be classified as a combination of type I (due to the N_2 uptake at low partial pressure suggesting a greater presence of micropores), and type IV (due to the presence of mesopores), which is evidenced by the prominent presence of hysteresis. Therefore, we can certainly state that both LS-derived carbons have their pore structures mainly composed of micro-meso pores. However, it is worthwhile to say that LS-C-1:4 adsorbed much

Table 1
Porosity characteristics of LS-C-1:2 and LS-C-1:4 samples.

	SSA	A_{Micro}	A_{Meso}	A_{Meso}	Pore volume
	(m^2/g)			(%)	(cm^3/g)
LS-C-1:2	1708	745	963	56.4	1.05
LS-C-1:4	2259	1055	1204	53.2	1.51

more N_2, which may certainly reflect in a higher specific surface area than LS-C-1:2.

The results proposed by N_2 adsorption-desorption isotherms are further evaluated through pore size distribution curves (Fig. 2b). In neither LS-derived carbons, the presence of big mesopores was recorded. Besides, small mesopores are seen in both LS-derived carbons, with LS-C-1:4 having the presence of more mesopores with sizes in the range of 2–4 nm, while LS-C-1:2 exhibited more activity in the range of microporosity with micropores sized at ~1.8 nm. Such differences in the pore sizes could cause an impact on their electrochemical performances since a high specific surface area and a great degree of mesoporosity can provide sufficient space and efficient transport channels for the Al-based charge carriers such as complex $AlCl_4^-$ anions [14,27].

From the N_2 adsorption-desorption isotherms, the specific surface area (SSA) values of the LS-C-1:2 and LS-C-1:4 samples were obtained (See Table 1). The SSA of both samples exhibited very high values, but LS-C-1:4 displayed a much higher value (2259 m^2/g) compared to LS-C-1:2 (1708 m^2/g). Such differences could be explained by the amount of KOH used in the activation process [28,29]. It is reported that increasing the amount of KOH leads to an increase in the SSA values of the carbon materials [28,29]. Highly porous structures can facilitate electron transfer and shorten ion transport pathways [27,30], thus boosting the electrochemical performance of the materials in terms of energy storage capacity. Further evaluating the pore features of the LS carbon materials, it can be seen that both have a well-balanced number of micro-mesoporosities, LS-C-1:2 contains 56.4 % of mesopores in its structure, while LS-C-1:4 has 53.2 %.

The LS-derived carbons were further evaluated by Raman spectroscopy (Fig. 2c), considering that crystalline graphitic structure or level of carbon lattice defects may affect properties/performances of the carbon materials when employed as electrode materials in batteries. Raman spectroscopy gives valuable insights into the degree of graphitization of the materials. Two important peaks can appear at around 1685 cm^{-1} (G band) that are related to in-plane stretching vibration of the sp^2 hybridized carbon atoms (planar carbon structure) and a second band around 1345 cm^{-1} (D band) that is attributed to the sp^3 C atoms (tetrahedral carbon structure), both peaks are present in both carbons. In addition, G' peak (2D peak) at 2688 cm^{-1} is observed in both carbons, but in the case of LS-C-1:2 it is much sharper. This peak indicates the properties of graphene and a very high degree of stacking. This suggests that increasing the amount of KOH led to a more disordered carbon lattice since the presence of graphene (highly ordered carbon atoms) is not present in LS-C-1:4. A ratio I_D/I_G can be obtained from these peaks, indicating the degree of graphitization of the LS carbons [31]. Fig. 2c shows that I_D/I_G of LS-C-1:2 is lower than LS-C-1:4, suggesting a lesser presence of defects in the LS-C-1:2 structure and more graphitic/crystalline structure [31]. It should be pointed out that carbon-based electrodes rich in defects can effectively work as electrodes because defects can act as active adsorption sites that help to boost the material's adsorptive properties and electrolyte penetration [32,33]. Fig. 2(d) shows the XRD patterns of LS-C-1:2 and LS-C-1:4. LS carbon shows a broad peak in the XRD pattern, indicating a predominantly amorphous structure [3]. The presence of graphitic domains within the LS carbon material is indicated by the peaks at around $2\theta = 26^\circ$ which corresponds to the (002) plane, and 2θ around 43° corresponding to the (1 0 1) plane [2,34–38]. These peaks suggest some degree of graphitization in the LS carbon materials in agreement with the Raman inferences.

Fig. 3 (a) to (c) are the TEM images of LS-C-1:2, and Fig. 3 (d) to (f) are the TEM images of LS-C-1:4. TEM images revealed the presence of both amorphous and graphitic layers. The graphitic layers appear as fringes with regular spacings for both the samples. However, the sample LS-C-1:2 seems to display a much more graphitized structure with the

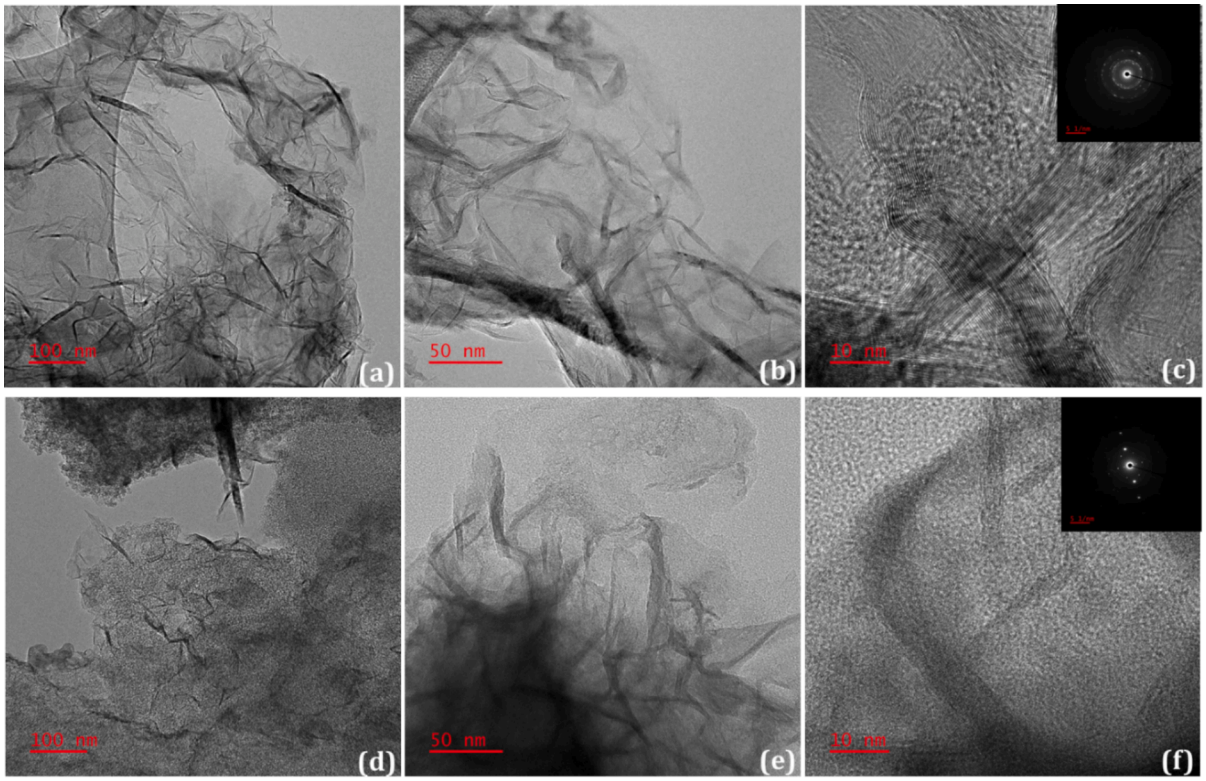

Fig. 3. (a) to (c) TEM images of LS-C-1:2 and (d) to (f) TEM images of LS-C-1:4.

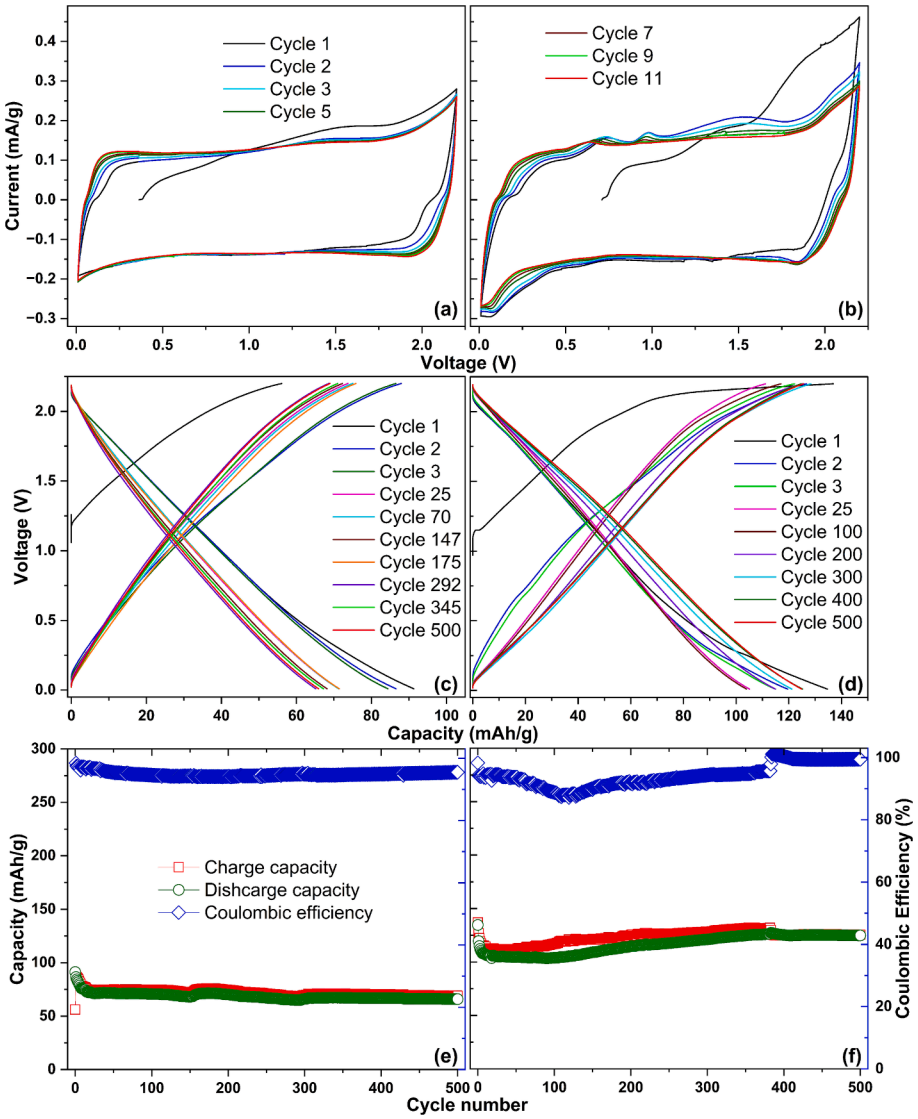

Fig. 4. CV profiles of (a) LS-C-1:2 and (b) LS-C-1:4; charge–discharge curves of (c) LS-C-1:2 and (d) LS-C-1:4 at 0.1 A/g current density; cycling behavior of (e) LS-C-1:2 and (f) LS-C-1:4 at 0.1 A/g current density.

presence of graphene sheets all over its structure, suggesting the increasing KOH amount reflects in the enhancement of the amorphousness of the lignin-based carbon material. The selected area electron diffraction (SAED) pattern of LS-C-1:2 revealed a clear ring with 6 bright spots (Fig. 3(c), insert image). These bright spots are related to the crystalline structure, connected to graphite in LS-C-1:2, which disappeared in LS-C-1:4 (Fig. 3(f)). This feature implies the absence or low concentration of long-range order in the carbon atomic lattice of LS-C-1:4.

3.2. Electrochemical analysis of the LS-derived carbons

The two cathode materials with different pore structures were evaluated for their electrochemical performances. The CV was conducted to explore the charge storage mechanism. Fig. 4 (a) and (b) are the CV curves for different cycles for LS-C-1:2 and LS-C-1:4, respectively. Both carbons showed no diffusion or intercalation peaks, a pseudocapacitive behavior with cathodic and anodic currents forming quasi-rectangular shapes. Unlike graphite/graphene, the LS carbons lack ordered structure and are unable to show (de)intercalation of charge carriers, $AlCl_4^-$ anions. Electrochemical adsorption and desorption of the charge carriers onto the surfaces of LS carbons, as described in equations 1–3, is the primary charge storage mechanism. The CV features of LS carbons are in good agreement with various biomass-derived carbons reported, as referenced in Table 2. CV data of both the samples displayed overlapped curves with constant currents and are promising for stable performance. However, LS-C-1:4 showed slightly higher redox currents than LS-C-1:2, indicating higher capacities, as confirmed in Fig. 4 (c-f). Fig. 4 (c) and (d) are the charge–discharge characteristics of LS-C-1:2 and LS-C-1:4, respectively, at 0.1 A/g current rate. The charge and discharge curves of both LS-derived carbons are found to be continuous sloping type in tune with the CV curves. These curves are found identical throughout the cycling, signifying that the charge storage mechanism is unchanged. The first cycle CV and charging curves are different because of the effects of initial electrolyte percolation and active electrode/electrolyte interface formation. Both LS-C-1:2 and LS-C-1:4 cathodes showed very good cycling performance at 100 mA/g as shown in Fig. 4 (e) and (f), but the later showed a trend of increasing capacities. It may be noted that in some instances, the coulombic efficiency of the LS-C-1:4 cathode slightly exceeded 100 %. This anomaly may arise due to several factors, including unexpected chemical reactions such as electrolyte decomposition or gas evolution. The instability in coulombic efficiency could be attributed to the more amorphous structure of the LS-C-1:4 sample compared to the LS-C-1:2. Notably, the LS-C-1:4 sample

Table 2
Comparative electrochemical performance of various bio-based carbon materials as cathode materials in ABs.

Source	Synthesis Method and Morphology	Operating Potential(V)	Current Rate (mA/g)	Initial Discharge Capacity (mA h/g)	Capacity Retention (mA h/g)/ (Cycles)
LS-C-1:2 (This work)	Synthesized via a one-step pyrolysis activation process. With a 1:2 ratio (LS:KOH) and pyrolyzed with a heating rate of 10 °C/min for 1 h and under an inert atmosphere.	0.01–2.2	100	91	66 (500)
LS-C-1:2 (This work)	Synthesized via a one-step pyrolysis activation process. With a 1:2 ratio (LS:KOH) and pyrolyzed with a heating rate of 10 °C/min for 1 h and under an inert atmosphere.	0.01–2.2	1000	64	74 (7300)
LS-C-1:4 (This work)	Synthesized via a one-step pyrolysis activation process. With a 1:4 ratio (LS:KOH) and pyrolyzed with a heating rate of 10 °C/min for 1 h and under an inert atmosphere.	0.01–2.2	100	135	125 (500)
LS-C-1:4 (This work)	Synthesized via a one-step pyrolysis activation process. With a 1:4 ratio (LS:KOH) and pyrolyzed with a heating rate of 10 °C/min for 1 h and under an inert atmosphere.	0.01–2.2	1000	70	91 (7300)
Sucrose [14]	Sucrose was carbonized over customized silica template particles and washed with NaOH etching. The carbonization was carried out at 900 °C under H_2/Ar atmosphere.	0.01–2.25	500	82	70 (1000)
Tar pitch [14]	The reaction mixture of tar pitch and KOH (1:4 wt%) was heated at 850 °C to produce activated carbon (AC). The porosity of AC is further modified by heat treatment at 750 °C under N_2 flow.	0.01–2.25	500	51	95 (1000)
CMK-3 [14]	–	0.5–2.3	980	~27	33 (36,000)
Birch sawdust [14]	Carbonized birch sawdust (400 °C) activated with 4 wt% of NaOH under Ar flow at 600–850 °C.	0.0–2.5	283	82	69 (40)
Coconut shell [14]	coconut shell chars were activated with 5 wt% of KOH at 850 °C under Ar atmosphere.	0.01–2.2	1000	90	81 (1500)
Human Hair [14]	Hair samples brunt at 300 °C were activated with 2 wt% of NaOH at 750 °C in Ar flow.	0.2–2.45	50	103	100 (50)
P-0 [39]	Pomegranate peel carbonized at 900 °C under Ar atmosphere. 0 min of ball milling.	0.01–2.4	200	100	80 (200)
P-5 [39]	Pomegranate peel carbonized at 900 °C under Ar atmosphere. 5 min of ball milling.	0.01–2.4	200	150	125 (200)
P-10 [39]	Pomegranate peel carbonized at 900 °C under Ar atmosphere. 10 min of ball milling.	0.01–2.4	200	169	90 (200)
Graphene [2]	Graphene prepared with high-pressure wet-jet milling (GWJM) of graphite in NMP solvent	0.5–2.41	1000	57	72 (10000)
meFLG [13]	few-layered graphene (meFLG) by exfoliating graphene oxide with microwave irradiation	0.5–2.41	1000	54	65 (10000)
N, S-C900 [40]	C_3N_4 –derived layered N,S heteroatom-doped carbon	0.01–2.25	500 5000	410.8 111	330 (500) 90 (10000)
NGF [41]	Hydrothermal treatment of silica nanosphere dispersed into graphene oxide solution	0.5–2.45	1000	137	133 (100)
G-SnS_2 [42]	3D reduced graphene oxide-supported SnS_2 nanosheets hybrid	0.4–2.10	100 200	392 –	– 70 (100)
FLG nanosheets [43]	Surface-perforated graphene (SPG) material by thermal reductive perforation of few-layer graphene nanosheets	0.5–2.4	5000	148	147 (1000)

exhibited a significantly higher discharge capacity compared to the low surface area counterpart LS-C-1:2 as shown in Table 2. LS-C-1:4 delivered the first discharge capacity of 135 mAh/g that retained up to ~93 % (125 mAh/g, Fig. 4(f)) at the end of the 500th cycle whereas corresponding values of LS-C-1:2 are found as 91 mAh/g and ~73 % only (66 mAh/g, Fig. 4(e)).

$$\textbf{Anode}: Al + 7\,AlCl_4^- \leftrightharpoons 4\,Al_2Cl_4^- + 3\,e^- \quad (1)$$

$$\textbf{Cathode}: C_n[AlCl_4] + e^- \leftrightharpoons C_n + AlCl_4^- \quad (2)$$

$$\textbf{Net Reaction}: Al + 4AlCl_4^- + 3\,C_n[AlCl_4] \leftrightharpoons 4\,Al_2Cl_7^- + 3\,C_n \quad (3)$$

The long-term cycling of both LS-derived carbons at 1.0 A/g current rate and subsequent rate capabilities with varying current rates are shown in Fig. 5. The charge and discharge curves of both LS carbons (Fig. 5(a-b)) are found to be similar to the 0.1 A/g cases, but the curves are more identical, and the symmetry between them increased with the cycling progressed. The straight line-like curves resemble the ideal supercapacitor-like behavior. Fig. 5 (b) and (d) show the cycling performance of LS-C-1:2 and LS-C-1:4 about 7000 cycles of continuous charge-discharges at 1.0 A/g current density, respectively. LS-C-1:2 delivered a discharge capacity of 64 mAh/g that slightly increased to 74 mAh/g at the 7300th cycle, whilst LS-C-1:4 showed a similar trend with 70 and 91 mAh/g for the first and 7300th discharges, respectively. Notably, Coulombic efficiencies (CEs) are found at ~ 100 % throughout the cycling in both cases, unlike their 0.1 mA/g current rate cycling. At high current rates, surface transportation of the charge carriers occurs very fast, evading plausible diffusion [13,37]. The capacity increase could be ascribed to the in-situ electrochemical exfoliation of graphitic regions seen in the XRD analysis [13]. The performance comparison between LS-C-1:2 and LS-C-1:4 w.r.t. their BET-specific surface area demonstrated that the porosity attributes of the cathodes significantly influenced their electrochemical metrics. The higher specific surface area and a porous structure are crucial for enhancing the contact area between the electrolyte and the active material. This facilitated faster ion percolation and improved the accessibility of $AlCl_4^-$ anions to the active sites, thereby boosting the battery's performance. For this reason, LS-C-1:4 exhibited superior performance than LS-C-1:2; however, later, one found better than some of its class of materials, as mentioned in Table 2. Additionally, both the LS carbon electrodes delivered impressive rate capabilities that maintained CEs greater than 98 % for LS-C-1:2 and around 100 % for LS-C-1:4 at all current rates tested, as seen in Fig. 5 (e) and (f), respectively. Specifically, even after the long-term cycling with 1.0 A/g, LS-C-1:2 delivered discharge capacities of 88, 75, 66, 59, 54, 49, 74 and 89 mAh/g at 0.1, 1.0, 2.0, 3.0, 4.0, 5.0, 1.0 and 0.1 A/g current densities respectively (Fig. 5(e)) whilst the respective capacities for LS-C-1:4 are recorded as 105, 89, 80, 72, 67, 63, 90 and 105 mAh/g (Fig. 5(f)). The biomass material often contains a conductive carbon network that enhances electrical conductivity and structural stability. This network helps to mitigate volume changes during the intercalation and deintercalation processes, maintaining the integrity of the electrode and ensuring long-term cycling stability. Overall, ABs with LS carbon cathodes demonstrated superior capacities and impressive cycling stability over 7000 cycles than some of their class of reported materials, including commercial materials such as graphene [2] and CMK-3 [14], as summarized in Table 2.

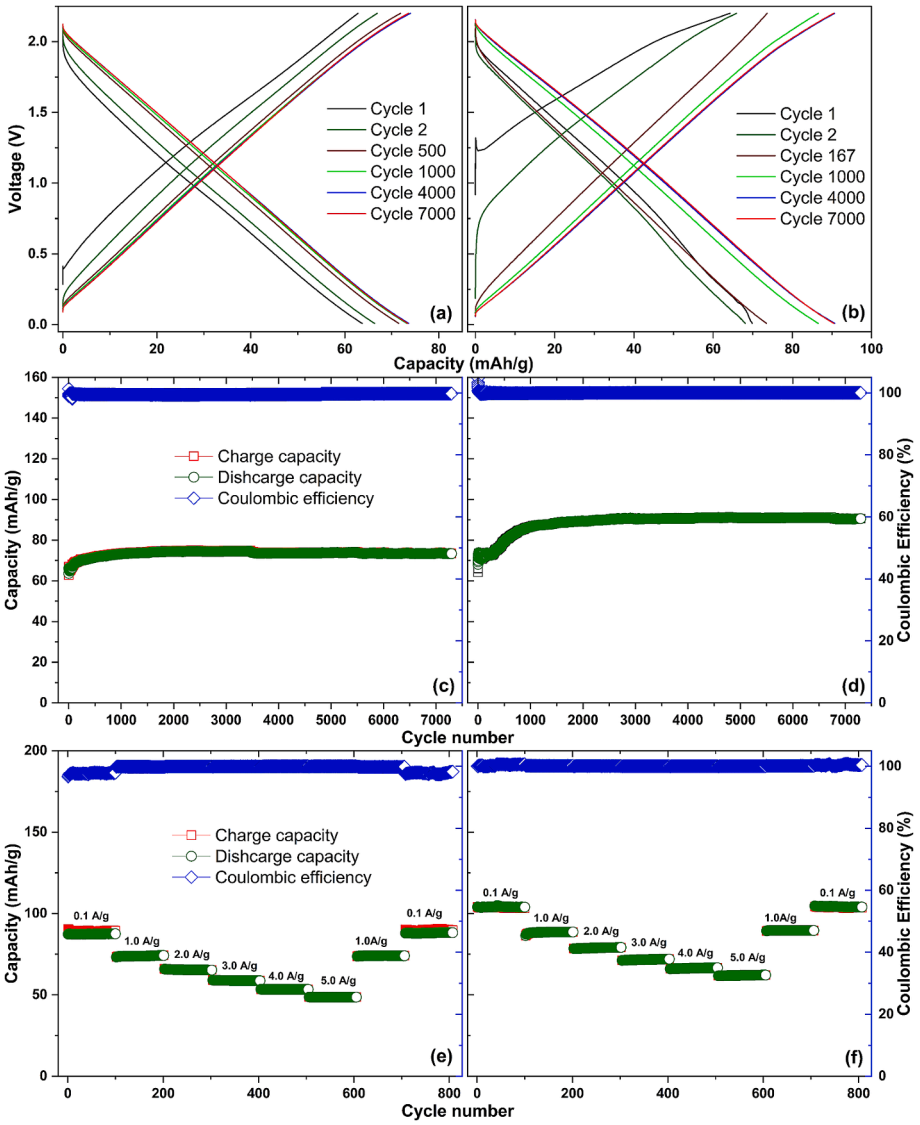

Fig. 5. Charge-discharge curves of (a) LS-C-1:2 and (b) LS-C-1:4 at 1.0 A/g current density; long-term cycling of (c) LS-C-1:2 and (d) LS-C-1:4 at 1.0 A/g current density; rate capability of (e) LS-C-1:2 and (f) LS-C-1:4.

The electrochemical data strongly suggest that the LS-derived carbons used as cathodes for ABs performed excellently. Although the nature of every carbon-based cathode material is different, and each cathode has its own merits and demerits, we propose a reliable comparison of the data generated in this work with other similar cathode materials reported globally (see Table 2). In addition, it is taken into consideration that the values reported in Table 2 were acquired through their respective best-optimized conditions. As a result, it can be seen that the mesoporous carbon (derived from LS) cathodes exhibited the highest specific capacities and stability compared to the works listed in Table 2. For instance, LS-C-1:4 gave the highest capacity with the cathode made from pomegranate peel carbonized at 900 °C under Ar atmosphere and 5 min of ball milling [39]. Both P-5 and LS-C-1:4 samples delivered 125mAh/g. However, it is worth mentioning that this value was kept after 500 cycles for LS-C-1:4 while P-5 was at the end of 200 cycles for carbon derived from pomegranate peel. Furthermore, LS-C-1:4 presented better performance than all other carbon materials exhibited in Table 2, suggesting an excellent strategy to turn an abundant and low-cost carbon resource into valuable energy storage materials.

XRD and Raman scattering analyses (Fig. 6) are carried out on fresh and cycled LS-derived carbon electrodes to investigate any structural, defect, and phase changes during the charge–discharge process. The XRD patterns of the LS-C-1:2 (Fig. 6(a)) and LS-C-1:4 (Fig. 6(b)) electrodes showed the appearance of several similar small diffraction peaks after the first charge and discharge cycle. These diffraction peaks continued to appear even after 7000 charge–discharge cycles. The (002) graphitic peak and nearby peaks were not properly resolved in the case of fresh electrode, but after first charge, these peaks were clearly discernable in line with the several graphite and graphene materials [2,13,44]. These peaks were observed even after the first discharge and after subsequent discharges irreversible and stable structural evolution upon the first insertion of $AlCl_4^-$ anions. The appearance of these peak indicates that both the LS-derived carbons have several short-range graphene layers or basal planes those readily undergoes realignments into (100), (101) and other diffraction peaks after the first charging, i.e. upon $AlCl_4^-$ insertion [2,13,44]. Overall, between the both electrodes, only minor changes were noted in the XRD patterns, except for the peaks that emerged due to the intercalation of $AlCl_4^-$ anions in strong agreement with the reported graphitic materials [2,13,44] Fig. 6 (c) and 6 (d) show the Raman spectra of the LS-C-1:2 and LS-C-1:4 fresh electrodes and after different charge–discharge cycles, respectively. From the Raman spectra, it is evident that both the carbon materials have retained the characteristic G and D bands and there is no significant change in their positions, even after the 7000 charge and discharge cycles. This

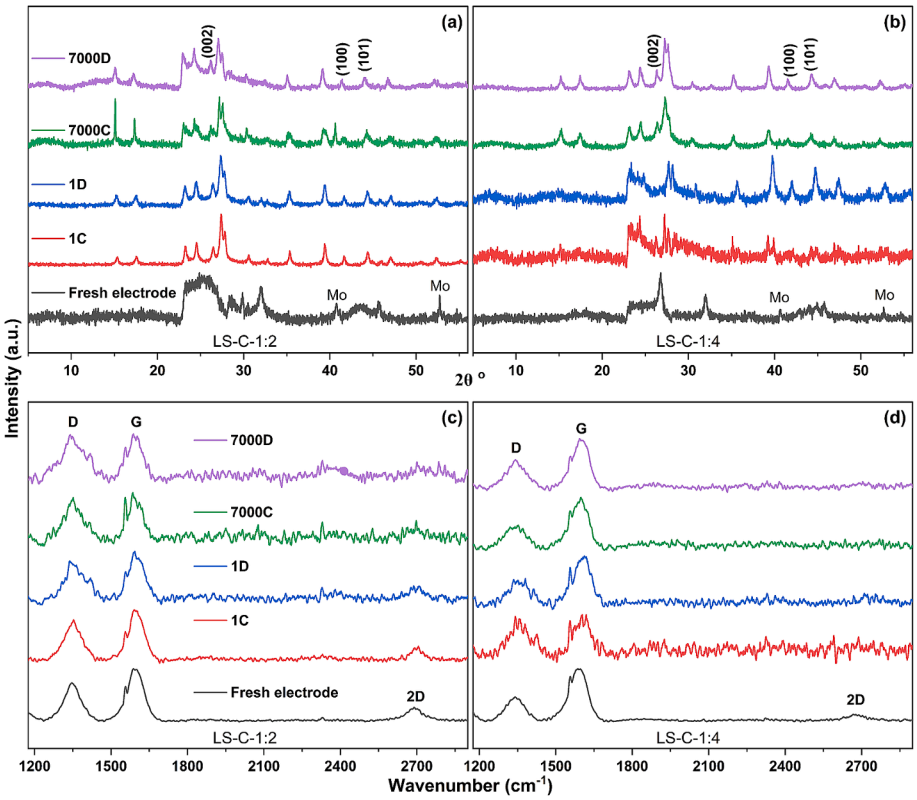

Fig. 6. XRD patterns of fresh and cycled (a) LS-C-1:2 and (b) LS-C 1:4 electrodes, and Raman spectra of fresh and cycled (c) LS-C-1:2 and (d) LS-C 1:4 electrodes.

shows that the 2D graphitic structure of the LS-derived carbons are intact during and after the electrochemical process. There is a very small blue shift in the spectra after cycling, which can be due to the intervention of foreign materials from the electrolyte and/or because of the stress during the electrochemical reactions during the charge–discharge process. However, in the case of LS-C-1:4 electrode, the intensity of the 2D band gradually decreased with charge–discharge cycles while other bands remained intact, implying that in this case basal plane stacking in the graphenaceous particles has slightly deteriorated [2,13,38,44]. Further, the intensity of D band of LS-C-1:2 gradually increased with the cycling and eventually matched with the G band whilst it found almost intact in the case of LS-C-1:4. This means that the 2D chemical nature of LS-C-1:2 is more susceptible to deterioration i.e. allows more defects compared to its counterpart. This is plausibly because of the lower amount of KOH (1:2) used that resulted in lower extent of the LS activation. All in all, XRD and Raman scattering analyses confirm that the structure of the LS-derived carbonaceous materials is a stable in the given electrochemical conditions.

4. Conclusion

In conclusion, the development and application of mesoporous carbon derived from lignin sulfonate as cathodes in ABs present a significant advancement in the field of aluminium battery technology. This study has demonstrated that lignin sulfonate, a renewable and abundant biomass resource, can be effectively converted into high-performance mesoporous carbon that is suitable as cathodes in aluminium batteries. The LS-C-1:4 exhibited more suitable physicochemical properties for $AlCl_4^-$ anions intercalation such as a higher specific surface area and mesopores compared to the LS-C-1:2. The LS-C-1:4 displayed a superior electrochemical performance by displaying a specific capacitance of 91 mAh/g at 1000 mA/g for 7300 cycles with almost 100 % of CE, which are higher metrics than many reported materials such as graphene and commercial activated carbons. The high specific surface area and amount of suitable mesoporous structure of LS-C-1:4 facilitated the ion transport and electron conductivity, thereby enhancing the overall electrochemical performance of the batteries. The findings indicate that the synthesized high specific surface and mesoporous carbon cathodes are suitable candidates for ABs with a high specific capacity, high rate capability, and prolonged cycling stability, which are critical parameters for the practical deployment of aluminium batteries in various energy storage applications. Moreover, the sustainable and cost-effective nature of lignin sulfonate as a precursor material aligns well with the growing demand for environmentally friendly and economically viable energy storage solutions.

CRediT authorship contribution statement

Fathima Ali Kayakool: Writing – review & editing, Writing – original draft, Methodology, Funding acquisition, Formal analysis, Data curation. **Harita Pant:** Writing – review & editing, Writing – original draft, Methodology, Formal analysis, Data curation. **Menestreau Paul:** Writing – review & editing, Writing – original draft, Formal analysis, Data curation. **Glaydson Simões Dos Reis:** Writing – review & editing, Writing – original draft, Resources, Methodology, Investigation, Formal analysis, Data curation, Conceptualization. **Gopinathan Manavalan:** Formal analysis, Data curation. **Venkata Satya Siva Srikanth Vadali:** Writing – review & editing, Writing – original draft, Supervision, Investigation, Formal analysis. **Mikael Thyrel:** Writing – review & editing, Writing – original draft, Validation, Supervision, Investigation. **Shaikshavali Petnikota:** Writing – review & editing, Writing – original draft, Validation, Supervision, Resources, Methodology, Investigation, Formal analysis, Data curation, Conceptualization.

Declaration of competing interest

The authors declare that they have no known competing financial interests or personal relationships that could have appeared to influence the work reported in this paper.

Acknowledgment

This research was funded by Bio4Energy - a Strategic Research Environment appointed by the Swedish government and the Swedish University of Agricultural Sciences. Fathima Ali Kayakool thanks the Prime Minister's Research Fellows scheme for providing research fellowship and support to travel to Sweden. Dr. Glaydson dos Simoes Reis gratefully acknowledges financial support from the Research Council of Finland (Academy Research Fellows 2024, Project: Bio-Adsorb&Energy, grant no. 361583). Fathima Ali Kayakool and Prof. Dr.-Ing. Vadali are thankful to UoH-IoE by MHRD (Grant Number: F11/9/2019-U3(A)) for financial support.

References

[1] B. Scrosati, J. Hassoun, Y.-K. Sun, Lithium-ion batteries, A Look Future, Energy Environ. Sci. 4 (9) (2011) 3287–3295.
[2] S. Petnikota, D. Koch, M. Imran, J. Buha, J.K. Panda, M. Akbari Garakani, L. Marasco, A. Gamucci, F. Bonaccorso, V. Pellegrini, Spray-coated few-layer graphene as an aluminium battery cathode, Sustainable Energy Fuels 6 (18) (2022) 4311–4321.
[3] S. Petnikota, R. Chua, K.M. Boopathi, R. Satish, F. Bonaccorso, V. Pellegrini, M. Srinivasan, An insight into the electrochemical activity of Al-doped V_2O_3, J. Electrochem. Soc. 167 (10) (2020) 100514.
[4] J. Ni, W. Li, H. Li, X. Huo, S. Xiao, Simple Cu^{2+} modification significantly improves the electrochemical performance of MXene ($Ti_3C_2T_x$) in aluminum batteries, J. Electroanal. Chem. 953 (2024) 118000.
[5] D.-Y. Wang, C.-Y. Wei, M.-C. Lin, C.-J. Pan, H.-L. Chou, H.-A. Chen, M. Gong, Y. Wu, C. Yuan, M. Angell, Y.-J. Hsieh, Y.-H. Chen, C.-Y. Wen, C.-W. Chen, B.-J. Hwang, C.-C. Chen, H. Dai, Advanced rechargeable aluminium ion battery with a high-quality natural graphite cathode, Nat. Commun. 8 (1) (2017) 14283.
[6] M.-C. Lin, M. Gong, B. Lu, Y. Wu, D.-Y. Wang, M. Guan, M. Angell, C. Chen, J. Yang, B.-J. Hwang, H. Dai, An ultrafast rechargeable aluminium-ion battery, Nature 520 (7547) (2015) 324–328.
[7] S. Wang, K.V. Kravchyk, F. Krumeich, M.V. Kovalenko, Kish graphite flakes as a cathode material for an aluminum chloride–graphite battery, ACS Appl. Mater. Interfaces 9 (34) (2017) 28478–28485.
[8] Y. Cai, S. Kumar, R. Chua, V. Verma, D. Yuan, Z. Kou, H. Ren, H. Arora, M. Srinivasan, Bronze-type vanadium dioxide holey nanobelts as high performing cathode material for aqueous aluminium-ion batteries, J. Mater. Chem. A 8 (25) (2020) 12716–12722.
[9] P. Wang, Z. Chen, H. Wang, Z. Ji, Y. Feng, J. Wang, J. Liu, M. Hu, J. Fei, W. Gan, Y. Huang, A high-performance flexible aqueous Al ion rechargeable battery with long cycle life, Energy Storage Mater. 25 (2020) 426–435.
[10] S. Wang, K.V. Kravchyk, S. Pigeot-Rémy, W. Tang, F. Krumeich, M. Wörle, M. I. Bodnarchuk, S. Cassaignon, O. Durupthy, S. Zhao, C. Sanchez, M.V. Kovalenko, Anatase TiO_2 nanorods as cathode materials for aluminum-ion batteries, ACS Appl. Nano Mater. 2 (10) (2019) 6428–6435.
[11] S.K. Das, Graphene, A cathode material of choice for aluminum-ion batteries, Angew. Chem., Int. Ed. 57 (51) (2018) 16606–16617.
[12] S. Petnikota, G. Dos Reis, F.A. Kayakool, V.V.S.S. Srikanth, J. Välikangas, U. Lassi, M. Thyrel, Elucidation of Electrochemical Performance of Few-Layered Graphene As Aluminium Battery Cathode Material: Effect of the Common O and S Impurities, ECS Meeting Abstracts MA2023-02 (8) (2023) 3328.
[13] S. Petnikota, G. Simões Dos Reis, F.A. Kayakool, V.S.S.S. Vadali, J. Välikangas, U. Lassi, M. Thyrel, Microwave exfoliated few-layered graphene cathode for aluminum batteries, ACS Appl. Energy Mater. 7 (16) (2024) 6862–6872.
[14] G.S. Reis, S. Petnikota, C.M. Subramaniyam, H.P. de Oliveira, S. Larsson, M. Thyrel, U. Lassi, F. García Alvarado, Sustainable biomass-derived carbon electrodes for potassium and aluminum batteries: conceptualizing the key parameters for improved performance, Nanomaterials 13 (4) (2023) 765.
[15] C. Zhang, R. He, J. Zhang, Y. Hu, Z. Wang, X. Jin, Amorphous carbon-derived nanosheet-bricked porous graphite as high-performance cathode for aluminum-ion batteries, ACS Appl. Mater. Interfaces 10 (31) (2018) 26510–26516.
[16] J.M. Rosas, R. Berenguer, M.J. Valero-Romero, J. Rodríguez-Mirasol, T. Cordero, Preparation of different carbon materials by thermochemical conversion of lignin, Front. Mater. 1 (2014) 29.
[17] R. Kumar Mishra, B. Singh, B. Acharya, A comprehensive review on activated carbon from pyrolysis of lignocellulosic biomass: an application for energy and the environment, Carbon Resour. Convers. 7 (4) (2024) 100228.
[18] N. Alwadani, P. Fatehi, Synthetic and lignin-based surfactants: challenges and opportunities, Carbon Resour. Convers. 1 (2) (2018) 126–138.
[19] M. Mennani, M. Kasbaji, A. Ait Benhamou, A. Boussetta, A.A. Mekkaoui, N. Grimi, A. Moubarik, Current approaches, emerging developments and functional prospects for lignin-based catalysts – a review, Green Chem. 25 (8) (2023) 2896–2929.
[20] Y. He, Y. Yang, X. Ye, Y. Lv, Y. Liu, M. Liu, Enhanced persulfate activation for sulfadiazine degradation by N, S self-doped biochar from sludge and sulfonated lignin: emphasizing the roles of graphitic nitrogen and thiophene sulfur, J. Environ. Chem. Eng. 12 (3) (2024) 112407.
[21] G. Simões dos Reis, C. Mayandi Subramaniyam, A.D. Cárdenas, S.H. Larsson, M. Thyrel, U. Lassi, F. García-Alvarado, Facile synthesis of sustainable activated biochars with different pore structures as efficient additive-carbon-free anodes for lithium- and sodium-ion batteries, ACS Omega 7 (46) (2022) 42570–42581.
[22] G. Simões dos Reis, D. Bergna, S. Tuomikoski, A. Grimm, E.C. Lima, M. Thyrel, N. Skoglund, U. Lassi, S.H. Larsson, Preparation and characterization of pulp and paper mill sludge-activated biochars using alkaline activation: a box–behnken design approach, ACS Omega 7 (36) (2022) 32620–32630.
[23] G.S. dos Reis, S.H. Larsson, M. Mathieu, M. Thyrel, T.N. Pham, Application of design of experiments (DoE) for optimised production of micro- and mesoporous Norway spruce bark activated carbons, Biomass Convers. Biorefin. 13 (11) (2023) 10113–10131.
[24] G.S. dos Reis, R.M.A. Pinheiro Lima, S.H. Larsson, C.M. Subramaniyam, V.M. Dinh, M. Thyrel, H.P. de Oliveira, Flexible supercapacitors of biomass-based activated carbon-polypyrrole on eggshell membranes, J. Environ. Chem. Eng. 9 (5) (2021) 106155.
[25] B. Long, F. Wu, Y. Li, H. Yang, W. Liu, Y. Li, Q. Li, X. Feng, Y. Bai, C. Wu, Manipulating the corrosion homogeneity of aluminum anode toward long-life rechargeable aluminum battery, Carbon Neutralization 3 (1) (2024) 64–73.
[26] M. Thommes, K. Kaneko, A.V. Neimark, J.P. Olivier, F. Rodriguez-Reinoso, J. Rouquerol, K.S.W. Sing, Physisorption of gases, with special reference to the evaluation of surface area and pore size distribution (IUPAC, Technical Report) 87 (9–10) (2015) 1051–1069.
[27] P. Thanwisai, N. Chaiyapo, P. Phuenhinlad, Y. Kanaphan, J. Nash, C. Chotsuwan, A. Klamchuen, Y. Wang, T. Nann, N. Meethong, Mesoporous and defective activated carbon cathode for $AlCl_4^-$ anion storage in non-aqueous aluminium-ion batteries, Carbon 191 (2022) 195–204.
[28] Y. Zhang, Y.-P. Zhao, L.-L. Qiu, J. Xiao, F.-P. Wu, J.-P. Cao, Y.-H. Bai, F.-J. Liu, Insights into the KOH activation parameters in the preparation of corncob-based microporous carbon for high-performance supercapacitors, Diam. Relat. Mater. 129 (2022) 109331.
[29] R.L. Zornitta, K.M. Barcelos, F.G.E. Nogueira, L.A.M. Ruotolo, Understanding the mechanism of carbonization and KOH activation of polyaniline leading to enhanced electrosorption performance, Carbon 156 (2020) 346–358.
[30] Y. Wang, R. Liu, Y. Tian, Z. Sun, Z. Huang, X. Wu, B. Li, Heteroatoms-doped hierarchical porous carbon derived from chitin for flexible all-solid-state symmetric supercapacitors, Chem. Eng. J. 384 (2020) 123263.
[31] G.S. dos Reis, J. Thivet, E. Laisné, V. Srivastava, A. Grimm, E.C. Lima, D. Bergna, T. Hu, M. Naushad, U. Lassi, Synthesis of novel mesoporous selenium-doped biochar with high-performance sodium diclofenac and reactive orange 16 dye removals, Chem. Eng. Sci. 281 (2023) 119129.
[32] Y. Xu, X. Sun, Z. Li, L. Wei, G. Yao, H. Niu, Y. Yang, F. Zheng, Q. Chen, Boosting the K+-adsorption capacity in edge-nitrogen doped hierarchically porous carbon spheres for ultrastable potassium ion battery anodes, Nanoscale 13 (46) (2021) 19634–19641.
[33] E. Laisné, J. Thivet, G. Manavalan, S. Petnikota, J.-P. Mikkola, M. Thyrel, T. Hu, E. C. Lima, M. Naushad, U. Lassi, G.S. dos Reis, Box-Behnken design for the synthesis optimization of mesoporous sulfur-doped carbon-based materials from birch waste: promising candidates for environmental and energy storage application, Colloids Surf. A Physicochem. Eng. Asp. 692 (2024) 133899.
[34] H. Maseed, S. Petnikota, V.V.S.S. Srikanth, N.K. Rotte, M. Srinivasan, F. Bonaccorso, V. Pellegrini, M.V. Reddy, A new insight into Li-staging, in-situ electrochemical exfoliation, and superior Li storage characteristics of highly crystalline few-layered graphene, J. Energy Storage 41 (2021) 102908.
[35] S. Petnikota, N.K. Rotte, M.V. Reddy, V.V.S.S. Srikanth, B.V.R. Chowdari, MgO-Decorated few-layered graphene as an anode for Li-ion batteries, ACS Appl. Mater. Interfaces 7 (4) (2015) 2301–2309.
[36] S. Petnikota, N.K. Rotte, V.V.S.S. Srikanth, B.S.R. Kota, M.V. Reddy, K.P. Loh, B.V. R. Chowdari, Electrochemical studies of few-layered graphene as an anode material for Li ion batteries, J. Solid State Electrochem. 18 (4) (2014) 941–949.
[37] S. Petnikota, V.V.S.S. Srikanth, J.J. Toh, M. Srinivasan, C.V.R. Bobba, S. Adams, M. V. Reddy, Electrochemistry-related aspects of safety of graphene-based non-aqueous electrochemical supercapacitors: a case study with MgO-decorated few-layer graphene as an electrode material, New J. Chem. 43 (25) (2019) 9793–9801.
[38] S. Petnikota, H. Maseed, V.V.S.S. Srikanth, M.V. Reddy, S. Adams, M. Srinivasan, B. V.R. Chowdari, Experimental elucidation of a graphenothermal reduction mechanism of Fe_2O_3: an enhanced anodic behavior of an exfoliated reduced

graphene oxide/Fe_3O_4 composite in Li-ion batteries, J. Phys. Chem. C 121 (7) (2017) 3778–3789.
[39] B. Wang, Z. Zhang, F. Yuan, D. Zhang, H. Sun, H. Wang, J. Wang, Q. Wang, Z. Li, Synergistic effect of pore structure and crystalline domains enabling high capacity toward non-aqueous rechargeable aluminum batteries, J. Phys. Chem. Solid 179 (2023) 111394.
[40] J. Li, J.K. El-Demellawi, G. Sheng, J. Björk, F. Zeng, J. Zhou, X. Liao, J. Wu, J. Rosen, X. Liu, H.N. Alshareef, S. Tu, Pseudocapacitive heteroatom-doped carbon cathode for aluminum-ion batteries with ultrahigh reversible stability, Energy Environ. Mater. 7 (5) (2024) e12733.
[41] X. Huang, Y. Liu, H. Zhang, J. Zhang, O. Noonan, C. Yu, Free-standing monolithic nanoporous graphene foam as a high performance aluminum-ion battery cathode, J. Mater. Chem. A 5 (36) (2017) 19416–19421.
[42] Y. Hu, B. Luo, D. Ye, X. Zhu, M. Lyu, L. Wang, An innovative freeze-dried reduced graphene oxide supported SnS_2 cathode active material for aluminum-ion batteries, Adv. Mater. 29 (48) (2017) 1606132.
[43] Y. Kong, C. Tang, X. Huang, A.K. Nanjundan, J. Zou, A. Du, C. Yu, Thermal reductive perforation of graphene cathode for high-performance aluminum-ion batteries, Adv. Funct. Mater. 31 (17) (2021) 2010569.
[44] G.A. Elia, I. Hasa, G. Greco, T. Diemant, K. Marquardt, K. Hoeppner, R.J. Behm, A. Hoell, S. Passerini, R. Hahn, Insights into the reversibility of aluminum graphite batteries, J. Mater. Chem. A 5 (20) (2017) 9682–9690.